

Mobility-Controlled Performance of Thick Solar Cells Based on Fluorinated Copolymers

Wentao Li,^{#,†} Steve Albrecht,^{#,‡} Liqiang Yang,[§] Steffen Roland,[‡] John R. Tumbleston,^{||} Terry McAfee,^{||} Liang Yan,[†] Mary Allison Kelly,[†] Harald Ade,^{*,||} Dieter Neher,^{*,‡} and Wei You^{*,†,§}

[†]Department of Chemistry, University of North Carolina at Chapel Hill, Chapel Hill, North Carolina 27599-3290, United States

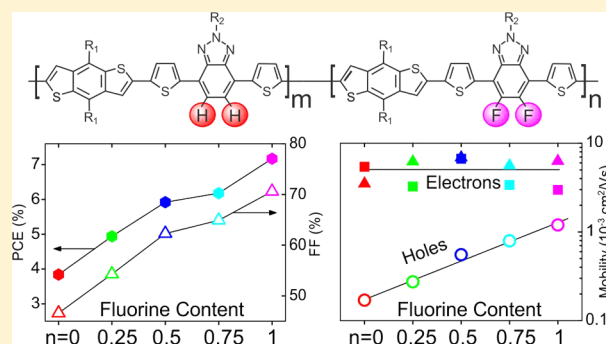
[‡]Institute of Physics and Astronomy, Soft Matter Physics, University of Potsdam, 14476 Potsdam, Germany

[§]Department of Applied Physical Sciences, CB #3216, University of North Carolina, Chapel Hill, North Carolina 27599-3216, United States

^{||}Department of Physics, North Carolina State University, Raleigh, North Carolina 27615, United States

S Supporting Information

ABSTRACT: Developing novel materials and device architectures to further enhance the efficiency of polymer solar cells requires a fundamental understanding of the impact of chemical structures on photovoltaic properties. Given that device characteristics depend on many parameters, deriving structure–property relationships has been very challenging. Here we report that a single parameter, hole mobility, determines the fill factor of several hundred nanometer thick bulk heterojunction photovoltaic devices based on a series of copolymers with varying amount of fluorine substitution. We attribute the steady increase of hole mobility with fluorine content to changes in polymer molecular ordering. Importantly, all other parameters, including the efficiency of free charge generation and the coefficient of nongeminate recombination, are nearly identical. Our work emphasizes the need to achieve high mobility in combination with strongly suppressed charge recombination for the thick devices required by mass production technologies.



INTRODUCTION

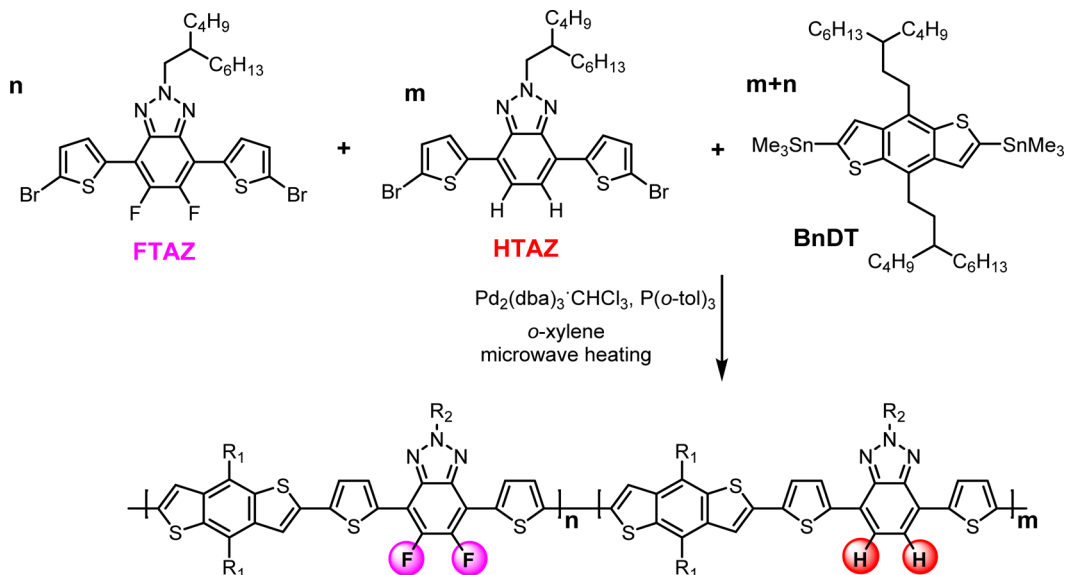
As a promising low cost energy conversion technology for a sustainable future, organic solar cells have received a tremendous amount of attention in the past decade. Intensive research activities into organic based donor (D):acceptor (A) bulk-heterojunction (BHJ) devices have generated rapid and significant progress, with 10% efficiency single active layer polymer:fullerene cells already on the horizon.¹ Though these impressive accomplishments have been largely driven by the design and synthesis of novel conjugated materials,^{2–6} pursuing a fundamental understanding of the complex donor:acceptor morphology^{7–9} and device physics^{10–12} of these novel materials has offered invaluable insights, providing important correlations between chemical structure and device properties. However, given the fact that many factors influence the photovoltaic performance of BHJ devices—chemistry/materials related properties (energy levels, band gap, molecular weight, etc.), morphology and molecular texture related properties (molecular orientation, domain size and purity, etc.), and charge carrier dynamics (yield and field-dependence of charge generation, nongeminate recombination, mobility, trapping etc.)—as-derived structure–properties correlations are typically convoluted.^{13,14} It has been very difficult, if at all possible, to draw simple and explicit correlations between a change in

chemistry and an observed variation in device performance, let alone offer straightforward yet convincing physical causes.

The complexity of such structure–function relations can be illustrated by the ongoing investigation of the “fluorine (F) effect”, i.e., the device performance improvement via the fluorine substitution into conjugated polymers.^{4,15–17} Indeed, a significant amount of work in pursuit of the underlying reasons for this “fluorine” effect has been carried out. While the often observed increase of the open circuit voltage (V_{oc}) is well understood and can be ascribed to the deeper HOMO (highest occupied molecular orbital) energy level of the fluorinated polymer,⁴ it became clear that fluorination can also increase other photovoltaic properties (but does not always do so), such as the short circuit current (J_{sc}) and the fill factor (FF).² Several mechanisms, such as charge separation assisted by the intramolecular electrostatics,¹⁸ improvements in mobility due to planarization of the backbone along with better intermolecular order,¹⁹ preferential texture with respect to the substrate,¹⁷ and preferential orientation of the backbone with respect to the discrete D/A interface,⁹ have been proposed as explanations for the “F effect”. However, relating such structural

Received: July 9, 2014

Published: October 7, 2014

Scheme 1. Synthesis of the Set of PBnDT-(X)TAZ with Various Amount of F Substitution^a

^aR₁ = 3-butylnonyl, R₂ = 2-butyloctyl.

changes to device performance becomes difficult since altering the chemical structure of the backbone typically affects important morphological (e.g., domain size distribution and purity) and textural parameters (e.g., molecular packing and orientation). (For simplicity, we use the term “morphology” to describe the spatial distributions of the organic donor and acceptor, and “texture” to describe molecular packing, mosaicity, and orientation correlations.) For example, typical polymer:fullerene blend systems are characterized by a significant change in domain size and purity when fluorine atoms are added to the acceptor moiety of the “donor–acceptor” polymer.^{17,20–22} Importantly, these meso-scale morphological changes will affect other relevant parameters, such as the probability that a photogenerated exciton reaches the heterojunction of dispersed minority D or A, or that free carriers recombine nongeminately.²⁰ Furthermore, the molecular weight of these conjugated polymers has a significant, and only recently appreciated, impact on morphology and device performance,²³ but is not always well controlled.²⁴ Therefore, though several studies revealed a monotonic change of some or all photovoltaic parameters with increasing fluorine content,^{21,25,26} it turned out to be difficult to assign these chemical structure induced performance changes to basic physical processes and causes. Finally, these studies rarely quantified all loss processes. With a limited set of measurements, one can only reach incomplete conclusions.

In contrast to these earlier studies, where the impact of morphology and texture is significant and complicates the structure–property correlation, here we report that in a series of five PBnDT-FTAZ based copolymers² with a systematic increase of the F substitution and very comparable molecular weights, the morphology of the BHJ blends as well as molecular orientation of the polymer chains relative to the D/A interface is surprisingly similar for all five polymers blended with PCBM. However, the overall power conversion efficiency of these five closely structurally related polymers varies by more than 80%. A comprehensive investigation reveals that almost all parameters describing photocarrier dynamics are also comparable, except the hole mobility. In fact, the monotonic and steady

enhancement of hole mobility with the increasing F substitution on the conjugated backbone is solely responsible for the significantly increased fill factor, the dominant impact on the overall efficiency, of ~350 nm thick BHJ devices for these five copolymers. Almost all other previously proposed explanations for the “F effect” are either not observed or only play very minor roles in this study. We primarily attribute the increases in mobility to improved intermolecular charge transfer due to an observed improvement in the molecular π – π stacking in the beneficial face-on orientation relative to the electrodes.

Recent work has identified insufficient hole mobility as a major cause of limited device performance: inefficient hole extraction results in enhanced losses via nongeminate recombination.^{13,27} These effects become particularly important for large layer thicknesses, since photogenerated charges need to travel a large distance toward the electrodes and internal fields are rather low in the solar cell working regime and decrease with increasing layer thickness.^{28,29} Our discovery of this simple, yet unambiguous, correlation between carrier mobility and fill factor caused by the increased F substitution, urges us to search for methods to increase the charge carrier (e.g., holes) mobility, implementing both intentional molecular structure design and/or careful morphological control in the BHJ blend. Such an approach will enable high device efficiencies for active layer thickness above 300 nm, which is ideal for high absorption and ease of fabrication, particularly when considering roll-to-roll or other high volume printing techniques preferred for commercialization.

RESULTS

Design and Synthesis of PBnDT-(X)TAZ. We chose PBnDT-(X)TAZ to construct the studied set of copolymers, because the hydrogen version (PBnDT-HTAZ) and the fluorinated version (PBnDT-FTAZ) have shown significant differences in important device characteristics in thick film devices.^{2,9} The amount of fluorine (F) substitution in the PBnDT-(X)TAZ was systematically varied by adjusting the feed ratio of these two monomers (HTAZ and FTAZ) via random

Table 1. PBnDT-(X)TAZ: Chemical Composition, Molecular Weight, and Photovoltaic Device Properties

PBnDT-(X)TAZ ^a	feed ratio of HTAZ:FTAZ (wt % F) ^b	actual wt % F ^c	M_n (kg/mol)	dispersity (Đ)	V_{oc} (V)	J_{sc} (mA/cm ²)	FF (%)	η (%)
F00*	1:0 (0.00)	0.00	71	2.6	0.731 ± 0.004	11.27 ± 0.48	46.6 ± 0.9	3.84 ± 0.16
F25	3:1 (0.94)	0.93	59	2.9	0.742 ± 0.001	12.27 ± 0.25	54.3 ± 0.7	4.94 ± 0.16
F50	1:1 (1.86)	1.77	44	2.5	0.764 ± 0.002	12.44 ± 0.37	62.3 ± 1.0	5.92 ± 0.22
F75	1:3 (2.77)	2.45	44	2.7	0.780 ± 0.004	12.21 ± 0.36	64.9 ± 1.3	6.18 ± 0.25
F100*	0:1 (3.66)	3.35	38	2.5	0.797 ± 0.004	12.75 ± 0.44	70.6 ± 1.3	7.17 ± 0.32

^aNomenclature: “F25” represents the polymer made with a feed ratio of HTAZ:FTAZ at 3:1, thus 25% FTAZ by molar ratio in (X)TAZ. The wt % F in the polymer, however, is actually 0.93%, as given in the column entitled with “actual % F”. “*” denotes a homopolymer (i.e., “F00” is the original PBnDT-HTAZ, and “F100” is the original PBnDT-FTAZ). ^bTheoretical wt % F is the calculated value based on the feed ratio of HTAZ:FTAZ. ^cActual wt % F was obtained by elemental analysis of all five samples. Note that there must be a slight systematic error that underreports the actual F-content, as even the F100 yields a value below what is expected.

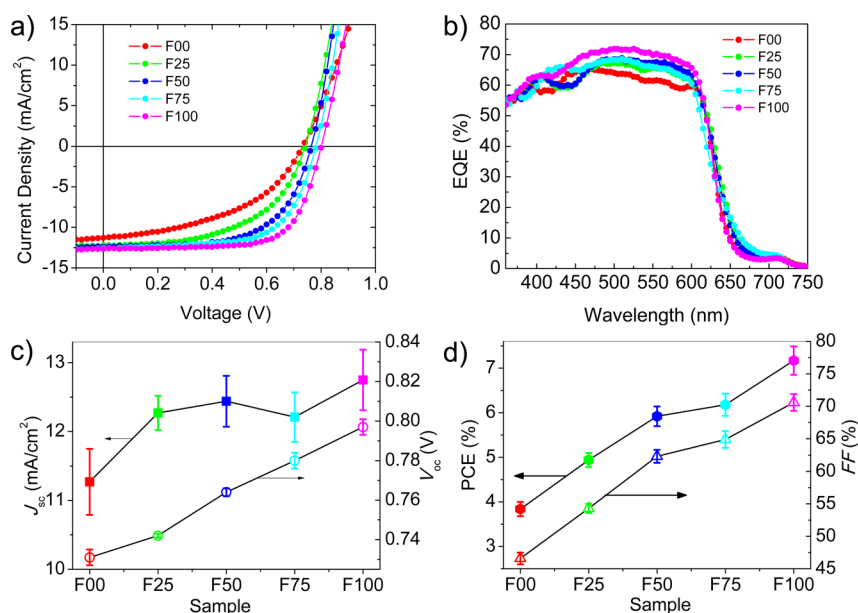


Figure 1. (a) J - V curves for the BHJ devices of ~ 350 nm thick films based on all five copolymers of PBnDT-(X)TAZ under 1 sun, AM 1.5G condition. (b) EQE for the same devices in (a). (c) The change of J_{sc} and V_{oc} with increased amount of F substitution. (d) The increase of fill factor tracks the increase of overall device efficiency as more F substituents are incorporated into the copolymer.

copolymerizations (Scheme 1 and Table 1). Since the only difference between these two monomers (HTAZ and FTAZ) is the two fluorine substituents on the central benzotriazole, and all polymers were prepared via (random) polycondensation, this set of polymers can be considered to be PBnDT-HTAZ with $x\%$ of randomly selected HTAZ units, on the conjugated backbone, substituted with two F atoms (i.e., no regular pattern; 0% is the original PBnDT-HTAZ while 100% is the original PBnDT-FTAZ).

Obtaining such a set of conjugated polymers, differing only on the amount of F substitution in a random fashion, is not a simple task. For example, two previous investigations^{24,26} on a similar set of polymers based on PTB7 with different amount of F substitution (0% to 100% in 20% increments) obtained different device results, and therefore reached different conclusions, largely because of the poor control of the molecular weight. In addition, the actual F% in the copolymers significantly deviated from the expected value derived from the feed ratio.²⁴ Fortunately, we recently demonstrated that with purified monomers and catalysts, the molecular weight of PBnDT-FTAZ can be precisely controlled via the classic Carothers equation.²³ Furthermore, by correlating molecular weight with device performance, we showed that a number-

average molecular weight (M_n) of 40 kg/mol appears to be optimal for fully achieving the excellent photovoltaic properties of PBnDT-FTAZ.²³ We thus followed our previously reported procedure to carefully purify all monomers (i.e., FTAZ, HTAZ and BnDT), catalyst, and other reagents, and applied stoichiometric control methods to achieve similar molecular weights for this set of PBnDT-(X)TAZ polymers. Indeed, the measured molecular weights of all four F-containing polymers (i.e., F25 through F100) are around 40 kg/mol, except for F00 (i.e., the original PBnDT-HTAZ) which has a higher molecular weight of 71 kg/mol. Overall, there is an anticorrelation, with lower molecular weight achieved for higher F-content. This is likely due to the lower solubility of fluorinated conjugated polymers, which could cause retention of the low molecular weight fraction in the final polymer during the Soxhlet extraction (thus a lower overall molecular weight). Importantly, the actual amount of F substitution in these copolymers, determined by elemental analysis, matches the calculated amount (from the feed ratio of HTAZ:FTAZ) exceedingly well (Table 1), a clear indication of the “randomness” of these copolymerizations. The optical and aggregation properties of these polymers are quite similar and consistent with prior observations, with the absorption coefficient increasing slightly

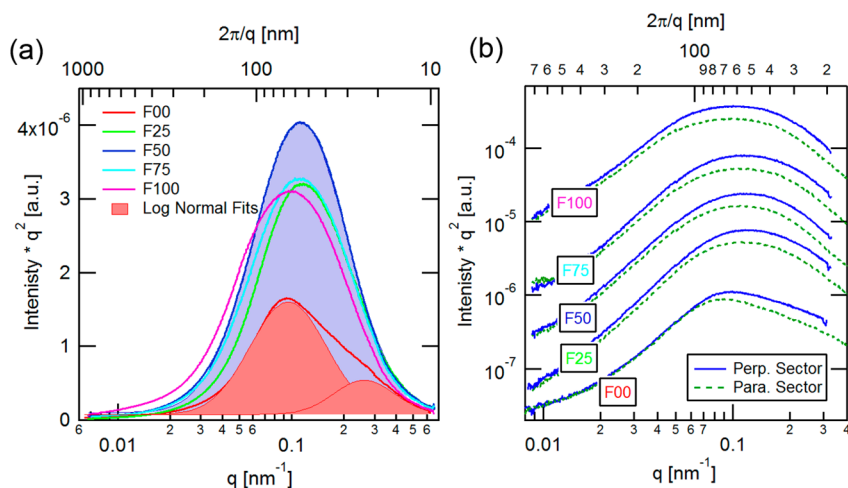


Figure 2. (a) P-SoXS circular average profiles at 284.1 eV. Scattering profiles for all blends show similar intensity and shape, indicating similar distributions of spatial frequencies along with composition variations in the samples. All blends can be fitted with single log-normal distributions, except for the F00 blend, which requires two for a good fit. (b) Sector averaged profiles representing P-SoXS data perpendicular and parallel to the electric field polarization. All samples show greater scattering perpendicular to the electric field, reflecting face-on preferential molecular orientation with respect to D/A interfaces (for data as a function of energy and quantitative analysis, see Figure S10).

as more F substituents were added on the conjugated backbone (Figure S1, Supporting Information). In addition, the HOMO energy levels estimated from the CV measurement are quite similar to less than 0.1 eV difference among all five copolymers (Figure S2), with the F00 (i.e., PBnDT-HTAZ) being the highest and the F100 (i.e., PBnDT-FTAZ) the lowest as previously reported (supplementary Table S1).

Photovoltaic Device Properties. Photovoltaic properties of these polymers were obtained via standard BHJ devices fabricated with identical processing condition (see Experimental Section for more details) in order to minimize impact on the PV performance from other factors (e.g., morphological changes due to different solvent, current variation due to significant difference in the thickness of active layer). Here, we chose an active layer thickness of ~ 350 nm, which is of significant commercial relevance, in particular for roll-to-roll printing. All thicknesses were very similar, with less than 5% difference from one copolymer to the other (see Table S2). Only through these rigorous controls can one draw meaningful conclusion about structure–property relationships.

Figure 1a displays the J – V curves under 1 sun condition (AM 1.5G, 100 mW/cm^2) for all devices, with corresponding external quantum efficiency (EQE) presented in Figure 1b. With the data tabulated in Table 1, we plot the open circuit voltage (V_{oc}), short circuit current (J_{sc}), fill factor (FF) and the overall efficiency (η) against the amount of F substitution (%), as shown in Figure 1c,d. A few notable findings emerge. First, the V_{oc} almost linearly increases with the amount of F substitution. This implies that the electronic states/orbitals, particularly the HOMOs, are delocalized and averaged over many monomer units, likely due to the random nature of the F substitution. However, the difference of V_{oc} between F00 and F100 is only 0.07 V, corresponding to a less than 10% increase going from F00 to F100. Second, it appears that there is a large increase in J_{sc} when 25% of the HTAZ being substituted with FTAZ (i.e., F25), but then the increase of J_{sc} due to further increasing the amount of F substitution levels off (with a slight fluctuation). Still, going from F00 to F100, the J_{sc} only increases about 13%. Importantly, the current generated for high reverse bias almost merges for all blends (Figure S4), demonstrating

that the dependence of J_{sc} on chemical structure is mainly coupled to the fill factor. The fill factor, not only shows a gradual increase along with the amount of F substitution, it exhibits the most significant change of all parameters, with an improvement of about 50% going from F00 to F100. Overall, and synergistically, the device efficiency steadily improves as the amount of F substitution increases, resulting in an 80% enhancement, from F00 (less than 4% overall energy conversion efficiency) to F100 (over 7% efficiency). Notably, the gradual increase in the device efficiency by incorporating more F substitution tracks the trend of the fill factor extremely well (Figure 1d), clearly reflecting that the fill factor is the dominant factor for the efficiency enhancement.

In order to understand the cause(s) responsible for the significantly improved efficiency, fill factor in particular, a detailed investigation of the morphology and device physics was needed and was therefore undertaken.

Morphology and Molecular Texture. The differences in performance described above could be due to changes in morphology with sequential fluorination of the conjugated backbone. Indeed, fluorination has been shown to modify morphology^{17,20} and could be an important effect in this system as well. However, as shown below, similar active layer morphologies were observed for all devices in this work.

First, polarized resonant soft X-ray scattering (P-SoXS) reveals that the domain spacing, domain purity, and preferential molecular orientation with respect to the D/A interfaces cannot explain the performance differences described above. Figure 2 shows Lorentz-corrected P-SoXS scattering profiles of active layer films floated directly from measured devices. The peak in scattering intensity, or long period, corresponds to domain spacings between 55 and 65 nm. Furthermore, the shapes of the scattering profiles are similar, indicating similar distributions of spatial frequencies of the samples. Specifically, BHJ blends based on F25 through F100 only exhibit one log-normal spatial frequency distribution as shown in Figure 2a. Only F00 requires two log-normal distributions to fit the observed spatial frequency distributions. Along with domain spacing, integration of each scattering profile represents the total scattering intensity (TSI), which is proportional to the square root of the average

composition variations over the length-scales characterized.⁷ Except for the F00 blend, all samples exhibit similar TSI and therefore similar average domain purities, which differ at most in a nonmonotonic way by 15%. The F00 blend has domains at two length scales that are on average 35% more mixed than the other blends. The slightly different morphology for the F00 blend could be due to the higher molecular weight of the polymer in this blend. Finally, anisotropic scattering, the strength of which has been positively correlated in some systems to fill factor and J_{sc} ,⁹ was observed for all samples in this study, and corresponds to the beneficial face-on molecular orientation with respect to the D/A interfaces. The strength of molecular orientation is similar for the F25 to F100 samples, with differences being less than 10%. As with the domain purity, the F00 blend is also different in regard to this structural parameter. It exhibits a more random orientation relative to the D/A interface, which is marked by the scattering anisotropy being 30% weaker and only observed for the high- q peak. We note that the HTAZ used in the current study has a higher molecular weight than in the prior work by Tumbleston et al.,⁹ in which the HTAZ exhibited nearly random molecular orientation, and thus a larger difference in molecular orientation with respect to FTAZ than in the current study. The prior work also exhibited a larger difference in performance, consistent with a possible impact arising from a difference in molecular orientation as postulated by Tumbleston et al. These differences emphasize again that molecular weight can impact morphology, aggregation, and texture. Detailed studies of all structural parameters and device physics are therefore required when assessing modifications of chemical structures.

Furthermore, FTAZ-based devices have been shown to be relatively insensitive to differences in morphology,³⁰ so long as the molecular weight is reasonably high.²³ It is thus unlikely that the relatively subtle and nonmonotonic changes that are observed in these morphological parameters can explain monotonic changes in the device performance. Especially since, except for the F00 blend, the morphologies of the four F-substituted blends (F25 through F100) are very similar and the differences that are observed do not correlate to the device performance. Thus, the interpretation of trends in the device data as a function of the amount of F substitution has to be based on parameters other than morphology (i.e., composition distributions) or molecular orientation relative to the D/A interface.

In contrast to the P-SoXS data that assesses the mesoscale morphology and the in-plane molecular orientation relative to the D/A interface, grazing incidence wide-angle X-ray scattering (GIWAXS), shows a clear and monotonic evolution of the texture, i.e., molecular packing and mosaicity (Figure 3). Even though overall, only broad (100) and (010) polymer peaks are observed, indicating short coherence lengths and a high degree of disorder,^{30,31} significant evolutions can be readily observed. Figure 3 clearly shows that an increase in the amount of F substitution causes a significant increase in overall (010) intensity, particularly in the out-of-plane direction (i.e., perpendicular to the electrodes). At the same time, the (100) spacing increases, and the lamellar stacking becomes increasingly in-plane. The latter is consistent with reoriented chains and crystallites that have face-on orientation with respect to the electrodes and thus enhance the out-of-plane π - π stacking. The increased π - π stacking might modify the average spacing in the (010) direction, thus forcing (due to volume conservation) the side chains to have, on average, a more

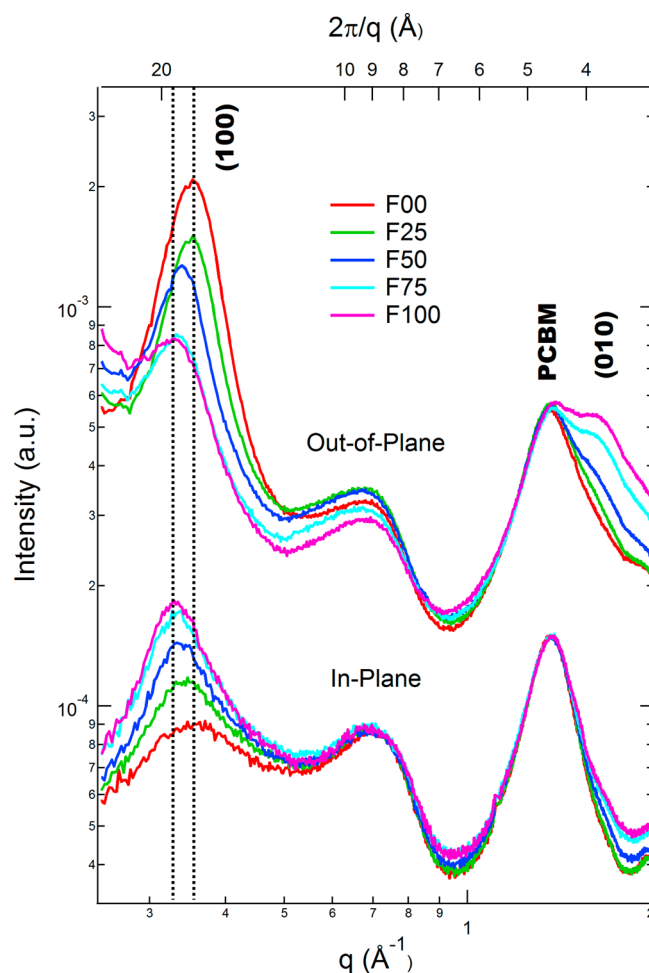


Figure 3. GIWAXS data of blend films on glass/ITO/PEDOT:PSS device substrates. The (100) lamellar, PCBM, and (010) π - π stacking peaks are labeled. π - π stacking intensity, face-on crystallite orientation with respect to the substrate, and lamellar distance increase with more fluorine content. In-plane and out-of-plane data set offset for clarity.

extended conformation along the lamellar direction, resulting in the increased lamellar spacing from F00 to F100 as observed. The GIWAXS data thus indicate a systematic evolution of molecular packing with increased π - π stacking, and increased beneficial face-on orientation relative to the electrodes as the amount of F substitution increases. This evolution improves intermolecular hole transfer in the required direction (vide infra). Additionally, the GIWAXS data clearly shows a PCBM aggregation peak at 1.4 \AA^{-1} , indicating that a favorable energetic landscape and good electron transport is also present for the electrons.

Factors Influencing Fill Factor. After having established that only minor morphological differences but trending texture exist for all five blends, we turn our attention to charge carrier dynamics in order to understand the pronounced increase in fill factor with the higher amount of F substitution in the conjugated backbone. The fill factor depends on three fundamental processes. The first process is the *charge generation efficiency*, meaning the probability that an incident photon generates a free charge at a given internal field. Some, but not all, studies have shown that the formation of free charge carriers depends on the field, since the initially geminate pairs need to overcome the Coulomb attraction. Therefore, a low charge generation efficiency can cause the fill factor of the device to

deteriorate.^{32,33} Second, the fill factor is affected by losses due to *nongeminate recombination* (NGR), i.e., the free charge that is lost due to recombination before being extracted. The NGR loss current density (J_{rec}) is proportional to the recombination coefficient γ multiplied by the steady state carrier density n to the power of the recombination order, which is two for bimolecular recombination (BMR). Therefore, in the case of BMR, this current loss can be expressed as $J_{\text{rec}} = e \cdot d \cdot \gamma \cdot n^2$ where e is the elementary charge and d the active layer thickness. When the recombination coefficient γ is high, e.g., due to low domain purity, free charges will be lost, particularly at low internal fields close to the V_{oc} which results in a reduced fill factor.³⁴ Third, when *charge extraction* is inefficient due to low (e.g., hole) mobilities, a higher overall steady-state carrier density n is present in the device. Therefore, the probability that a carrier undergoes NGR is increased,¹³ resulting again in a low fill factor. For a given generation current and electric field, the carrier density in the active layer scales inversely with mobility. Thus, since the nongeminate recombination loss is proportional to the product of electron and hole density, this loss is very sensitive to the mobility.

Recently, techniques have become available that can selectively probe losses from field dependent free charge formation and NGR.^{32,33} Time-delayed collection field (TDCF) is one of these techniques.³³ Within TDCF, a short laser pulse generates charge carriers at a certain applied bias (prebias V_{pre}), which is selected to lie within the solar cell working regime. After 10 ns, the voltage is ramped up to high reverse bias (collection bias V_{coll}) to extract all generated charges, thus avoiding losses from NGR. Importantly, the delay time of 10 ns between photogeneration and extraction ensures that all geminate pairs resulting in free charges have been split up before the collection bias is applied, and using low fluences ensures that losses due to NGR are suppressed during the short delay.

Charge Generation. The external generation efficiency (EGE) measured as a function of applied prebias for all five blends as determined by TDCF with a 530 nm excitation wavelength is displayed in the upper panel of Figure 4. As TDCF with properly selected parameters fully suppresses nongeminate losses, the EGE is a reliable measure of how efficiently incident photons are converted into extractable free charges as a function of external bias. Figure 4 (upper panel) clearly shows that the charge generation is independent of the applied field for all five blends studied in this work. As the formation of free charges occurs via the thermalized charge transfer (CT) states in a working solar cell,³⁵ the field-independent charge generation observed here hints at a sufficiently delocalized and only weakly bound CT state. This can be fulfilled in the presence of aggregated PCBM domains³⁶ when there also exists a favorable interfacial energy landscape that stabilizes charges away from the donor:acceptor interface.^{12,37}

To exactly quantify the efficiency of free charge generation and collection for the five polymer/PBCM blends, external quantum efficiency (EQE) spectra were recorded as a function of bias (Figure S4). At high reverse bias, losses from NGR are excluded and the EQE measured under these conditions gives the absolute yield of free charge formation and coincides with the EGE. Interestingly, for all five blends, the EQE at high reverse bias is very comparable, around 69–73%, with EQE reduced by only 3% for F00 (i.e., PBnDT-HTAZ) when compared with other blends. Together with the field

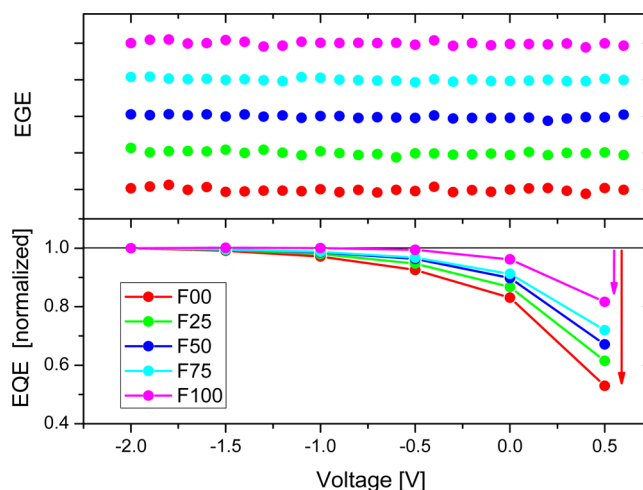


Figure 4. Upper panel: the external generation efficiency (EGE) offset for clarity as a function of applied prebias measured with TDCF at excitation wavelength of 530 nm. Lower panel: The EQE measured at 530 nm and normalized to -2 V as a function of voltage for all five blends. The arrows indicate the losses due to NGR at 0.5 V for F00 and F100.

independent charge generation in these blends, this observation suggests that the absolute efficiency of charge generation is very comparable for all blends at all fields. Therefore, at reduced bias, the drop in EQE must be due to NGR as we will discuss below.

Nongeminate Recombination. The lower panel in Figure 4 shows the field-dependent EQE extracted at 530 nm for direct comparison with the upper panel that displays the EGE. The EQE is normalized to a high reverse bias of -2 V. In contrast to the EGE, the EQE decreases with bias between 0 and 0.5 V, which is entirely caused by NGR (the relative NGR losses at 0.5 V is indicated by the arrows in Figure 4). This loss is largely reduced by the increased F substitution, which mirrors the increase in fill factor.

By varying the delay between charge generation and the extraction of all remaining free charges, the TDCF technique is able to track the fate of photogenerated free carriers. Data from these delayed extraction measurements for F50 at conditions close to the respective open circuit voltage are shown in Figure 5a, with the complete set of data for all five samples shown in Figure S5. The amount of collected charge (Q_{coll}) as a function of delay time can be fitted to a recombination model which also accounts for the number of charges that have been extracted during delay (Q_{pre}). By definition, Q_{coll} and Q_{pre} add up to Q_{tot} which is the total number of extractable charges. The data is best described when only bimolecular recombination (BMR) is included as the dominating nongeminate recombination mechanism for all five blends, meaning that the current loss due to NGR depends quadratically on the carrier density and is thus very sensitive to the extraction efficiency of the devices. Figure 5b shows the bimolecular recombination coefficient deduced from the fits at 0.7 V for all five blends. Interestingly, although the fill factor increases almost linearly with the amount of F substitution in the conjugated backbone, the BMR coefficient is virtually identical at around $1 \times 10^{-17} \text{ m}^3/\text{s}$ for all five blends. This mirrors the fact that the quantum efficiency of free charge generation is unaffected by fluorination, consistent with the picture that both processes involve the same intermediates. Our data on the BMR coefficient essentially

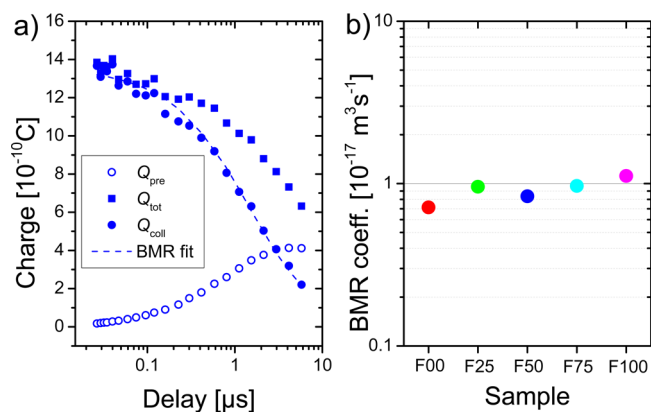


Figure 5. (a) The measured number of collected charges (Q_{coll}) and the corresponding bimolecular recombination (BMR) fit with increasing delay time between laser pulse and extraction voltage for the F50 sample at 0.7 V prebias. The number of charges that are extracted during delay is Q_{pre} . The sum of both, $Q_{coll} + Q_{pre} = Q_{tot}$ is the total amount of charges. (b) The BMR coefficient deduced from BMR fits as shown in (a) at conditions close to the respective open circuit for all five blends.

exclude a possible cause, a large change of the BMR coefficient, from accounting for the significantly different fill factor in this study. The very small effect of the increased fluorine substitution on the BMR coefficient in this study is consistent with the fact that the mesoscale morphologies are very similar for all five blends, but stands in contrast to previous results on fluorinated PCPDTBT, where the BMR coefficient was shown to decrease substantially upon fluorination.¹³ The decrease of BMR coefficient for fluorinated PCPDTBT was attributed to the formation of larger and purer phases, in accordance with earlier interpretations from recombination experiments and simulations.^{38,39} The weak change on the BMR coefficient found here can, therefore, be attributed to the fact that domain size and purity differ very little among all five blends.

Charge Extraction. Since we establish BMR as the dominating NGR mechanism in this study, the current density that is lost due to NGR will increase quadratically with carrier density. Consequently, even small increases in the steady state charge carrier density will speed up recombination losses. Because the overall steady state carrier density is directly impacted by the charge carrier mobilities, we performed a detailed study of the electron and hole mobility in all five blends. Electron and hole mobility were measured separately with different techniques and these results are compiled in Figure 6. Interestingly, electron mobilities deduced from the photocurrent transients in TDCF and those from the space charge limited current (SCLC) of electron-only devices compare very well. All five blends have similar values of around 5×10^{-3} cm²/V·s, which is quite typical for the electron mobility in well performing polymer:fullerene blends. In stark contrast, the SCLC hole mobility from the hole-only devices varies by a factor of 7, from 0.17×10^{-3} cm²/V·s in the case of F00 blend to 1.2×10^{-3} cm²/V·s for the F100 blend (see Figure S7 for more details).

To verify the impact of a lower hole mobility on the average steady state carrier density, we applied the bias enhanced charge extraction (BACE) technique recently introduced by the Neher lab.^{13,40} BACE is very comparable to TDCF with the only difference being the illumination conditions. With BACE, a laser diode is applied for milliseconds to realize steady state

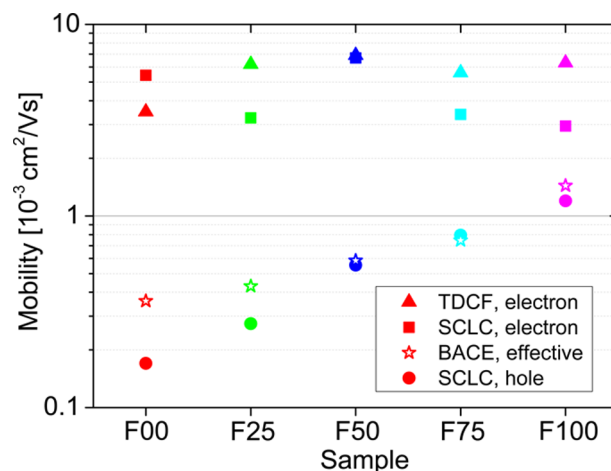


Figure 6. Charge carrier mobilities of electrons and holes together with the effective extraction mobility as a function of fluorine substitution. The electron mobility is deduced from the transit time of TDCF transients and from electron-only devices measured in the SCLC regime. The hole mobility is measured with hole-only devices in the SCLC regime, and the effective extraction mobility is determined via BACE as described in the text.

between generation, recombination, and extraction at each bias. Then the laser diode is switched off within 10 ns and the voltage is reversed to extract all charges without any loss during extraction. Therefore, BACE is able to measure the steady state carrier density present in the device. The results are presented in Figure S8. In the operating regime, with the light intensity adjusted to give a short circuit current of 14 mA/cm², the steady state carrier density decreases steadily with increased amount of F substitution for all operating voltages (Figure S8). Therefore, though the coefficient for BMR is almost the same for the five blends, the lower carrier density in the more fluorinated polymer based devices slows down NGR, resulting in a significant increase of the fill factor.

In addition to providing the average steady state carrier density under virtually all bias and illumination conditions, the BACE technique further offers the effective extraction mobility, which is a nonlinear function of the hole and the electron mobility as shown recently.¹³ In the working solar cell, charge carrier motion by drift or diffusion is driven by the gradient of the quasi Fermi levels.⁴¹ This gradient is calculated from the difference in voltage that is needed to establish a certain carrier density either at open circuit or in the operating regime. From this gradient, the overall carrier density, and the current that is generated at these conditions, the effective extraction mobility can be estimated, according to recently published methodology.¹³ The data obtained from this analysis is presented in Figure 6, which clearly shows that more fluorination increases the effective extraction mobility. Additionally, the comparison of the effective extraction mobility with the hole mobility deduced from SCLC measurements reveals that the steady state carrier density present in the device under illumination is strongly determined by the hole mobility.

To summarize the results of the charge carrier dynamics experiments, we find that the generation of free charge is field-independent and that the overall generation efficiency is very comparable for all blends studied. Furthermore, the BMR coefficient is equally moderate at ca. 1×10^{-17} m³/s and is not affected by fluorination. According to Langevin's recombination model, the recombination coefficient is directly proportional to

the sum of electron and hole mobility.⁴² Apparently, the BMR coefficient is determined by the faster type of carrier, the electrons, as the recombination coefficient and the electron mobilities are equally constant in our system. Calculating the Langevin recombination coefficient with the measured mobilities yields values around $3 \times 10^{-15} \text{ m}^3/\text{s}$ for the studied blends, meaning that BMR recombination is suppressed by a factor of 300–400 for all five blends. In contrast, similar studies on annealed P3HT:PCBM blends in the Neher lab revealed hole and electron mobilities (from TDCF transient fits) of 0.5×10^{-3} and $2 \times 10^{-3} \text{ cm}^2/\text{V}\cdot\text{s}$, respectively.⁴³ Together with a BMR coefficient of $0.5 \times 10^{-17} \text{ m}^3/\text{s}$ measured on the very same P3HT:PCBM blends, this gives a reduction factor of ca. 150. Thus, recombination is more strongly suppressed in the F100:PCBM blend than in the annealed P3HT:PCBM blend. We surmise that this low BMR is related to the very low fullerene miscibility observed for F00 and F100. Following prior procedures,³⁰ we find that only ~4% residual PCBM remains in either polymer (see Figure S9) after extensive solvent annealing in trichlorobenzene, which results in all the PCBM—which is in excess of the thermodynamic miscibility limit—crystallizing into macroscopic, large, and well separated crystals. Considering the overall quite amorphous, or highly disordered, nature of these polymers, this residual fullerene concentration is one of the lowest observed for all donor polymers studied to date.^{7,28,44} This reflects an inherently unfavorable molecular interaction between the fullerene and the polymers, thereby resulting in sufficiently pure domains in the corresponding BHJ blends.

A thermal annealing sequence over 40 min allows the average composition fluctuations of the unannealed blends used here to be put on an absolute scale.⁴⁴ The R-SoXS TSI and thus relative domain purity rapidly saturates after 5–10 min of annealing (see Figure S12). Assuming that this asymptotic limit of the purity corresponds to the thermodynamic miscibility limit, perfect phase separation with domains of 100% purity would only yield a TSI that is 8% higher than observed here. The composition variations, scaling with the square-root of TSI, of the unannealed blend can thus be deduced to correspond to a relative purity of ~85%. Given that the majority of the PCBM is agglomerated into nearly pure PCBM domains (due to the low molecular weight of the PCBM), this implies that the average PCBM concentration in the donor-rich phases, i.e., pure aggregated donor polymer and mixed domains, is at most 15%. Since the donor polymer is aggregated (as per UV–vis) yet only slightly ordered (as per GIWAXS), the morphology is likely very complex and includes at least three phases or extensive gradients in composition between the pure PCBM agglomerates and the pure donor polymer aggregates. Such a morphology has a complex electronic landscape which helps to guide the charges from the mixed domains to more pure domains. The mixed domains, or gradients, which must comprise a large volume fraction due to the pure ordering of the donor polymer, allow for effective exciton harvesting and the pure domains allow for effective transport with low bimolecular recombination. In short, the combination of the overall very high hole and electron mobilities and the strongly reduced recombination are the key aspects to achieve high fill factors (over 70%) for thick active layers of F100 based BHJ blends.

DISCUSSION

Several possible parameters, including morphology, backbone planarization, internal dipole moment change, etc., have been proposed to describe the impact of fluorination on the solar cell device performance. Given that the morphology is changing so little here, we have an ideal case to definitively investigate the impact of other parameters and further understand the “F effect”. The constancy of the UV–vis spectra (see Figure S1) directly suggests that backbone planarization is not an effect of fluorination in our system.¹⁹ Similarly, the similar field independent external charge generation efficiency (EGE) and bimolecular recombination for all materials definitively prove that the internal dipole moment change (between the ground state and the excited state)¹⁸ has no significant impact on the charge generation or suppression of recombination in our system. Similarly, molecular interactions and orbital overlap can be excluded as a cause here. We stress that such conclusions cannot be made if the only device data available, or utilized, are *J–V* characteristics; one should conduct comprehensive investigation on chemistry/materials, morphology, and device physics with a carefully designed and synthetically controlled set of materials.

After ruling out all other possible causes, we discover that a single parameter, the hole mobility, is responsible for the change of short circuit current and fill factor in thick polymer solar cells (over 300 nm) of the studied copolymers. Our results show that the most important parameter that determines the fill factor in this series of polymer:fullerene blends is the charge extraction efficiency, which we find is limited by the hole mobility. The strong increase of hole mobility with the increased amount of fluorine substitution enables quicker charge extraction to the electrodes, thereby reducing the overall steady state carrier density present in the device. As a result, the fill factor steadily increases from F00 to F100. Reduced recombination is also shown to be beneficial for high J_{sc} which is significantly enhanced when going from F00 to F25. The high electron and hole mobilities in combination with the strongly reduced bimolecular recombination coefficient (relative to Langevin’s limit) for F100 (i.e., PBnDT-FTAZ) are the key reason for the high fill factor of up to 72.9% for its devices with a thick active layer (over 300 nm), which is maintained even for thickness of about $1 \mu\text{m}$.²

Our results clearly indicate that the increased fluorination on the conjugated backbone, more specifically, on the acceptor moiety of the “donor–acceptor” copolymers, benefits the hole carrier mobility with a strikingly monotonic correlation observed in this series (Figure 6). Because similar morphologies, probed by P-SoXS, have been observed for all five BHJ blends, the increased hole mobility with further fluorination is likely due to improved interchain transport, supported by the improved (010) π – π stacking and face-on orientation observed by GIWAXS. Furthermore, because of the random nature of these three copolymers (i.e., F25, F50 and F75), our results indicate that the “fluorine (F) effect” is not limited to structurally well-defined alternating copolymers such as PBnDT-FTAZ and other F-containing polymers. Therefore, strategically incorporating F substitution should be an important design rationale in future molecular design of conjugated polymers for BHJ solar cells.

CONCLUSION

A few important conclusions emerge from this unequivocal mobility-controlled performance of BHJ solar cells with thick films. First, given the fact that electron mobility in polymer:fullerene BHJ solar cells can be relatively high (e.g., $\sim 5 \times 10^{-3}$ cm²/V·s in this study via both SCLC and TDCF), a comparably high hole mobility is needed to guarantee efficient charge extraction at low internal fields, which helps to reduce the NGR and improve the fill factor³⁴ (and the short circuit current). For example, the obtained SCLC hole mobility of 1.2×10^{-3} cm²/V·s and the strongly reduced BMR coefficient for the F100 based device is sufficient to sustain a high fill factor of over 70% with a thick active layer over 300 nm. However, given the hole mobility is still lower than the electron mobility, further enhancing the hole mobility could in principle increase the fill factor to over 80%⁴⁵ for thicker active layers, a value on par with that of inorganic solar cells (e.g., Si, GaAs, etc.).

Second, a high hole mobility is even more important for the more popular small band gap donor based BHJ devices. With an increase in solar light absorption due to their small band gap, these devices can generate more charge carriers than the polymers (band gap of ~ 2.0 eV) in this study. Therefore, the small band gap devices are more susceptible to the current loss from NGR, which scales with the product of the recombination coefficient and the charge density squared (vide supra). Unfortunately, these small band gap polymers typically have low hole mobilities, which cannot reconcile the conflict between the light absorption (mandating a thick film) and fast charge extraction (requiring a thinner film if the hole mobility is low). With only few exceptions,^{46,47} these small band gap polymers based solar cells typically reach their performance maximum at ~ 100 nm,^{3,4,16,28} since a thicker film would lead to significantly reduced fill factor (and also current) due to recombination. Therefore, optimizing charge carrier extraction while maintaining efficient generation and strongly suppressed nongeminate recombination at relatively thick layers (over 300 nm) should remain key challenges for future material design and device optimization.

Fast charge carrier extraction requires a high hole mobility, which appears to be linked with the polymer backbone oriented “face-on” toward the substrate according to our results. Recent results, in fact, revealed a strong dependence of the vertical mobility on the backbone orientation.⁴⁸ Though it is yet not clear how this goal can be achieved via rational molecular design, the present results reveal that small changes in the chemical structure are sufficient to induce a significant reorientation of the backbone toward the preferential “face-on” alignment.

These challenges facing donor polymers also apply to the ongoing efforts to find fullerene replacements, where mobility measurements could be used as a screening tool. Finally, the “ideal” materials for polymer solar cells should not only have small band gaps to maximize the light absorption (i.e., a potentially high J_{sc}) and balanced energy levels (i.e., a high V_{oc}); they should also have comparably high electron/hole mobilities ($> 1 \times 10^{-3}$ cm²/V·s) for fast charge extraction (i.e., reducing the carrier density) while exhibiting a suitable morphology in the BHJ blend to reduce the recombination coefficient well below the Langevin limit (possibly smaller than 1×10^{-17} m³/s) to achieve a high fill factor.⁴⁹ All these should be achieved with thick films for maximizing the efficiency and

more importantly, for the future roll-to-roll manufacturing of such polymer solar cells.

EXPERIMENTAL SECTION

All polymers were synthesized according to previously published methods.^{2,23} For solar cells, indium tin oxide (150 nm via sputtering with patterned shadow mask; $20 \Omega/\square^{-1}$; purchased from Thin Film Devices) coated glass substrates were ultrasonicated in DI water, acetone, and isopropanol for 15 min per cleaning solvent. The substrates were dried under a stream of nitrogen and subjected to the treatment of UV-Ozone (UVO Cleaner Model 42, Jelight Company, Inc.) for 30 min. A filtered dispersion of PEDOT:PSS in water (Baytron PH500) was then spun cast onto clean ITO substrates at 4000 rpm for 60 s and then baked at 140 °C for 10 min to give a thin film with a thickness of 40 nm. Blends of PBnDT-(X)FTAZ:PCBM (1:2 w/w, 12 mg/mL for polymer) were dissolved in 1,2,4-trichlorobenzene with heating at 120–140 °C for 6 h. Blend films were spincoated on PEDOT:PSS from the hot solution at an RPM between 400 and 600 for 60 s. The substrates were transferred into vacuum chamber immediately after spin-coating and then dried at reduced pressure (~ 5 mmHg) for 30 min. The devices were finished for measurement after thermal deposition of a 30 nm film of calcium and a 70 nm film of aluminum as the cathode at a base pressure of 1×10^{-6} mbar. There are 8 devices per substrate, with an active area of 12 mm² per device. Device characterization was carried out under AM 1.5G irradiation with the intensity of 100 mW/cm² (Oriol 91160, 300 W) calibrated by a NREL certified standard silicon cell. Current density versus voltage (J - V) curves were recorded with a Keithley 2400 digital source meter. The photovoltaic parameters are the average values measured from 8 devices with the standard deviations as error bars, the reported J - V curves (e.g., Figure 1a) under 1 sun are from the devices that have the closest values to the average values in the 8 devices. All fabrication steps after adding the PEDOT:PSS layer onto ITO substrate, and characterizations were performed in gloveboxes under nitrogen atmosphere (MBraun, Inc.). Film thicknesses were measured with an Alpha-Step D-100 Stylus Profiler (KLA-Tencor).

R-SoXS measurements were conducted at beamline 11.0.1.2 of the Advanced Light Source (ALS)⁵⁰ following previously established methods and protocols,^{7,51,52} by floating sections of blend films from actual devices used for current–voltage measurements onto silicon nitride windows. GIWAXS was carried out at beamline 7.3.3 of the ALS⁵³ following previous methods on actual devices used for electrical measurements.⁵²

TDCF³³ was measured with pulsed excitation from a diode-pumped, Q-switched Nd:YAG laser (NT242, EKSPILA) with 5,5 ns pulse duration and 500 Hz repetition rate. An Agilent 81150A pulse generator was used to apply the pre- and collection bias to the sample in combination with a home-built amplifier. The current through the device was measured via a 50 Ω resistor in series recorded with a Yokogawa DL9140 oscilloscope. The pulse generator was triggered via a fast photodiode (EOT, ET-2030TTL). To compensate the internal latency of the pulse generator, the laser pulses were delayed via a multimode fiber (LEONI, 85m). The pulse fluence was measured with a Ophir Vega power meter equipped with a photodiode sensor (PD300-UV).

BACE¹³ was measured with the same setup as TDCF except for the illumination source. In BACE a high power 1W, 445 nm laser diode (insaneware) with ~ 10 ns light switch-off time is used. The LED is operated at 100 Hz repetition rate with applying the light for 9 ms to the sample to reach steady state conditions. The light is coupled into a fiber (LEONI, 60 m) for high homogeneity of the light profile. After the light is off, the voltage is reversed to extract all carriers without recombination losses being the same as in TDCF.

Samples for TDCF and BACE were prepared following the same procedure used to fabricate the devices for J - V measurements, except that the former devices had a smaller active area that ensured low RC time constants in the transient experiments. Devices were encapsulated with 2 component epoxy resin and a glass lid prior to air exposure.

■ ASSOCIATED CONTENT

■ Supporting Information

General methods; UV–vis spectra, cyclic voltammograms, GPC curves, NMR spectra of all five polymers; detailed device data; field dependent EQE; BMR coefficient by TDCF; mobility extracted by TDCF transients, by SCLC and by BACE; molecular miscibility by scanning transmission X-ray microscopy (STXM), and scattering anisotropy by polarized resonant soft X-ray scattering (P-SoXS). This material is available free of charge via the Internet at <http://pubs.acs.org/>.

■ AUTHOR INFORMATION

Corresponding Authors

hwade@ncsu.edu

neher@uni-potsdam.de

wyou@unc.edu

Author Contributions

#W.L. and S.A. contributed equally.

Notes

The authors declare no competing financial interest.

■ ACKNOWLEDGMENTS

The authors acknowledge the following support for this collaborative research. W.L., Liqiang Y. and W.Y. were supported by Office of Naval Research (N000141110235, and N000141410221). M.A.K. and W.Y. were supported by a National Science Foundation CAREER award (DMR-0954280). Liang Y. and W.Y. were supported by a NSF SOLAR Grant (DMR-1125803). W.Y. is a Camille Dreyfus Teacher-Scholar. X-ray characterizations and analysis and manuscript contributions by J.R.T., T.M. and H.A. were supported by DOE, OS, BES, MSE (DE-FG02-98ER45737). R-SoXS data was acquired at beamline 11.0.1.2, GIWAXS data at beamline 7.3.3, and STXM data at 5.3.2.2⁵⁴ of the ALS, a National user facility supported by DOE (DE-AC02-05CH1123). A. L. D. Kilcoyne, A. Hexemer, C. Wang, and A. Young of the ALS (DOE) assisted with the measurements and provided instrument maintenance. S.A., S.R., and D.N. acknowledge funding from the BMBF within PVcomB (FKZ 03IS2151D) and the DFG within the Priority Program SPP 1355. We acknowledge Jona Kurpiers for the help with the TDCF setup.

■ REFERENCES

- (1) Liao, S.-H.; Jhuo, H.-J.; Cheng, Y.-S.; Chen, S.-A. *Adv. Mater.* **2013**, *25*, 4766.
- (2) Price, S. C.; Stuart, A. C.; Yang, L.; Zhou, H.; You, W. *J. Am. Chem. Soc.* **2011**, *133*, 4625.
- (3) Cabanetos, C.; El Labban, A.; Bartelt, J. A.; Douglas, J. D.; Mateker, W. R.; Fréchet, J. M. J.; McGehee, M. D.; Beaujuge, P. M. *J. Am. Chem. Soc.* **2013**, *135*, 4656.
- (4) Chen, H.-Y.; Hou, J.; Zhang, S.; Liang, Y.; Yang, G.; Yang, Y.; Yu, L.; Wu, Y.; Li, G. *Nat. Photonics* **2009**, *3*, 649.
- (5) Zhou, H.; Yang, L.; You, W. *Macromolecules* **2012**, *45*, 607.
- (6) Uy, R. L.; Price, S. C.; You, W. *Macromol. Rapid Commun.* **2012**, *33*, 1162.
- (7) Collins, B. A.; Li, Z.; Tumbleston, J. R.; Gann, E.; McNeill, C. R.; Ade, H. *Adv. Energy Mater.* **2013**, *3*, 65.
- (8) Hedley, G. J.; Ward, A. J.; Alekseev, A.; Howells, C. T.; Martins, E. R.; Serrano, L. A.; Cooke, G.; Ruseckas, A.; Samuel, I. D. W. *Nat. Commun.* **2013**, *4*, 2867.
- (9) Tumbleston, J. R.; Collins, B. A.; Yang, L.; Stuart, A. C.; Gann, E.; Ma, W.; You, W.; Ade, H. *Nat. Photonics* **2014**, *8*, 385.

- (10) Hoke, E. T.; Vandewal, K.; Bartelt, J. A.; Mateker, W. R.; Douglas, J. D.; Noriega, R.; Graham, K. R.; Fréchet, J. M. J.; Salleo, A.; McGehee, M. D. *Adv. Energy Mater.* **2013**, *3*, 220.
- (11) Proctor, C. M.; Albrecht, S.; Kuik, M.; Neher, D.; Nguyen, T. Q. *Adv. Energy Mater.* **2014**, *4*, 1400230.
- (12) Shoaee, S.; Subramaniam, S.; Xin, H.; Keiderling, C.; Tuladhar, P. S.; Jamieson, F.; Jenekhe, S. A.; Durrant, J. R. *Adv. Funct. Mater.* **2013**, *23*, 3286.
- (13) Albrecht, S.; Tumbleston, J. R.; Janietz, S.; Dumsch, I.; Allard, S.; Scherf, U.; Ade, H.; Neher, D. *J. Phys. Chem. Lett.* **2014**, *5*, 1131.
- (14) Collins, B. A.; Tumbleston, J. R.; Ade, H. *J. Phys. Chem. Lett.* **2011**, *2*, 3135.
- (15) Zhou, H.; Yang, L.; Stuart, A. C.; Price, S. C.; Liu, S.; You, W. *Angew. Chem., Int. Ed.* **2011**, *50*, 2995.
- (16) Dou, L.; Chen, C.-C.; Yoshimura, K.; Ohya, K.; Chang, W.-H.; Gao, J.; Liu, Y.; Richard, E.; Yang, Y. *Macromolecules* **2013**, *46*, 3384.
- (17) Stuart, A. C.; Tumbleston, J. R.; Zhou, H.; Li, W.; Liu, S.; Ade, H.; You, W. *J. Am. Chem. Soc.* **2013**, *135*, 1806.
- (18) Carsten, B.; Szarko, J. M.; Son, H. J.; Wang, W.; Lu, L.; He, F.; Rolczynski, B. S.; Lou, S. J.; Chen, L. X.; Yu, L. *J. Am. Chem. Soc.* **2011**, *133*, 20468.
- (19) Schroeder, B. C.; Huang, Z.; Ashraf, R. S.; Smith, J.; D'Angelo, P.; Watkins, S. E.; Anthopoulos, T. D.; Durrant, J. R.; McCulloch, I. *Adv. Funct. Mater.* **2012**, *22*, 1663.
- (20) Albrecht, S.; Janietz, S.; Schindler, W.; Frisch, J.; Kurpiers, J.; Kniepert, J.; Inal, S.; Pingel, P.; Fostiropoulos, K.; Koch, N.; Neher, D. *J. Am. Chem. Soc.* **2012**, *134*, 14932.
- (21) Zhang, M.; Guo, X.; Zhang, S.; Hou, J. *Adv. Mater.* **2014**, *26*, 1118.
- (22) Son, H. J.; Wang, W.; Xu, T.; Liang, Y.; Wu, Y.; Li, G.; Yu, L. *J. Am. Chem. Soc.* **2011**, *133*, 1885.
- (23) Li, W.; Yang, L.; Tumbleston, J. R.; Yan, L.; Ade, H.; You, W. *Adv. Mater.* **2014**, *26*, 4456.
- (24) He, X.; Mukherjee, S.; Watkins, S.; Chen, M.; Qin, T.; Thomsen, L.; Ade, H.; McNeill, C. R. *J. Phys. Chem. C* **2014**, *118*, 9918.
- (25) Liu, P.; Zhang, K.; Liu, F.; Jin, Y.; Liu, S.; Russell, T. P.; Yip, H.-L.; Huang, F.; Cao, Y. *Chem. Mater.* **2014**, *26*, 3009.
- (26) Wang, H.; Yu, X.; Yi, C.; Ren, H.; Liu, C.; Yang, Y.; Xiao, S.; Zheng, J.; Karim, A.; Cheng, S. Z. D.; Gong, X. *J. Phys. Chem. C* **2013**, *117*, 4358.
- (27) Beiley, Z. M.; Hoke, E. T.; Noriega, R.; Dacuna, J.; Burkhard, G. F.; Bartelt, J. A.; Salleo, A.; Toney, M. F.; McGehee, M. D. *Adv. Energy Mater.* **2011**, *1*, 954.
- (28) Bartelt, J. A.; Beiley, Z. M.; Hoke, E. T.; Mateker, W. R.; Douglas, J. D.; Collins, B. A.; Tumbleston, J. R.; Graham, K. R.; Amassian, A.; Ade, H.; Fréchet, J. M. J.; Toney, M. F.; McGehee, M. D. *Adv. Energy Mater.* **2013**, *3*, 364.
- (29) Peet, J.; Wen, L.; Byrne, P.; Rodman, S.; Forberich, K.; Shao, Y.; Drolet, N.; Gaudiana, R.; Dennler, G.; Waller, D. *Appl. Phys. Lett.* **2011**, *98*, 043301.
- (30) Tumbleston, J. R.; Stuart, A. C.; Gann, E.; You, W.; Ade, H. *Adv. Funct. Mater.* **2013**, *23*, 3463.
- (31) Rivnay, J.; Mannsfeld, S. C. B.; Miller, C. E.; Salleo, A.; Toney, M. F. *Chem. Rev.* **2012**, *112*, 5488.
- (32) Credgington, D.; Jamieson, F. C.; Walker, B.; Nguyen, T.-Q.; Durrant, J. R. *Adv. Mater.* **2012**, *24*, 2135.
- (33) Albrecht, S.; Schindler, W.; Kurpiers, J.; Kniepert, J.; Blakesley, J. C.; Dumsch, I.; Allard, S.; Fostiropoulos, K.; Scherf, U.; Neher, D. *J. Phys. Chem. Lett.* **2012**, *3*, 640.
- (34) Proctor, C. M.; Kuik, M.; Nguyen, T.-Q. *Prog. Polym. Sci.* **2013**, *38*, 1941.
- (35) Vandewal, K.; Albrecht, S.; Hoke, E. T.; Graham, K. R.; Widmer, J.; Douglas, J. D.; Schubert, M.; Mateker, W. R.; Bloking, J. T.; Burkhard, G. F.; Sellinger, A.; Fréchet, J. M. J.; Amassian, A.; Riede, M. K.; McGehee, M. D.; Neher, D.; Salleo, A. *Nat. Mater.* **2014**, *13*, 63.
- (36) Gélinas, S.; Rao, A.; Kumar, A.; Smith, S. L.; Chin, A. W.; Clark, J.; van der Poll, T. S.; Bazan, G. C.; Friend, R. H. *Science* **2014**, *343*, 512.

- (37) Yost, S. R.; Van Voorhis, T. J. *Phys. Chem. C* **2013**, *117*, 5617.
- (38) Hamilton, R.; Shuttle, C. G.; O'Regan, B.; Hammant, T. C.; Nelson, J.; Durrant, J. R. *J. Phys. Chem. Lett.* **2010**, *1*, 1432.
- (39) Groves, C.; Greenham, N. C. *Phys. Rev. B: Condens. Matter Mater. Phys.* **2008**, *78*, 155205.
- (40) Lange, I.; Kniepert, J.; Pingel, P.; Dumsch, I.; Allard, S.; Janietz, S.; Scherf, U.; Neher, D. *J. Phys. Chem. Lett.* **2013**, *4*, 3865.
- (41) Würfel, P. *Physics of Solar Cells: From Principles to New Concepts*; WILEY-VCH Verlag GmbH & Co. KGaA: Weinheim, 2005, <http://onlinelibrary.wiley.com/book/10.1002/9783527618545>.
- (42) Lakhwani, G.; Rao, A.; Friend, R. H. *Annu. Rev. Phys. Chem.* **2014**, *65*, 557.
- (43) Kniepert, J.; Schubert, M.; Blakesley, J. C.; Neher, D. *J. Phys. Chem. Lett.* **2011**, *2*, 700.
- (44) Ma, W.; Tumbleston, J. R.; Wang, M.; Gann, E.; Huang, F.; Ade, H. *Adv. Energy Mater.* **2013**, *3*, 864.
- (45) Guo, X.; Zhou, N.; Lou, S. J.; Smith, J.; Tice, D. B.; Hennek, J. W.; Ortiz, R. P.; Navarrete, J. T. L.; Li, S.; Strzalka, J.; Chen, L. X.; Chang, R. P. H.; Facchetti, A.; Marks, T. J. *Nat. Photonics* **2013**, *7*, 825.
- (46) Hu, X.; Yi, C.; Wang, M.; Hsu, C.-H.; Liu, S.; Zhang, K.; Zhong, C.; Huang, F.; Gong, X.; Cao, Y. *Adv. Energy Mater.* **2014**, DOI: 10.1002/aenm.201400378.
- (47) Li, W.; Hendriks, K. H.; Roelofs, W. S. C.; Kim, Y.; Wienk, M. M.; Janssen, R. A. J. *Adv. Mater.* **2013**, *25*, 3182.
- (48) Steyrlleuthner, R.; Di Pietro, R.; Collins, B. A.; Polzer, F.; Himmelberger, S.; Schubert, M.; Chen, Z.; Zhang, S.; Salleo, A.; Ade, H.; Facchetti, A.; Neher, D. *J. Am. Chem. Soc.* **2014**, *136*, 4245.
- (49) Proctor, C. M.; Love, J. A.; Nguyen, T.-Q. *Adv. Mater.* **2014**, *26*, 5957.
- (50) Gann, E.; Young, A. T.; Collins, B. A.; Yan, H.; Nasiatka, J.; Padmore, H. A.; Ade, H.; Hexemer, A.; Wang, C. *Rev. Sci. Instrum.* **2012**, *83*, 045110.
- (51) Collins, B. A.; Cochran, J. E.; Yan, H.; Gann, E.; Hub, C.; Fink, R.; Wang, C.; Schuettfort, T.; McNeill, C. R.; Chabiny, M. L.; Ade, H. *Nat. Mater.* **2012**, *11*, 536.
- (52) Yang, L.; Tumbleston, J. R.; Zhou, H.; Ade, H.; You, W. *Energy Environ. Sci.* **2013**, *6*, 316.
- (53) Hexemer, A.; Bras, W.; Glossinger, J.; Schaible, E.; Gann, E.; Kirian, R.; MacDowell, A.; Church, M.; Rude, B.; Padmore, H. *J. Phys.: Conf. Ser.* **2010**, *247*, 012007.
- (54) Kilcoyne, A. L. D.; Tyliszczak, T.; Steele, W. F.; Fakra, S.; Hitchcock, P.; Franck, K.; Anderson, E.; Harteneck, B.; Rightor, E. G.; Mitchell, G. E.; Hitchcock, A. P.; Yang, L.; Warwick, T.; Ade, H. *J. Synchrotron Radiat.* **2003**, *10*, 125.